



CHALMERS
UNIVERSITY OF TECHNOLOGY

Resonant inelastic soft x-ray scattering on LaPt_2Si_2

Downloaded from: <https://research.chalmers.se>, 2025-05-17 09:40 UTC

Citation for the original published paper (version of record):

John Mukkattukavil, D., Hellsvik, J., Ghosh, A. et al (2022). Resonant inelastic soft x-ray scattering on LaPt_2Si_2 . Journal of physics. Condensed matter : an Institute of Physics journal, 34(32). <http://dx.doi.org/10.1088/1361-648X/ac7500>

N.B. When citing this work, cite the original published paper.

PAPER • OPEN ACCESS

Resonant inelastic soft x-ray scattering on LaPt_2Si_2

To cite this article: Deepak John Mukkattukavil *et al* 2022 *J. Phys.: Condens. Matter* **34** 324003

View the [article online](#) for updates and enhancements.

You may also like

- [Multi-scale simulations of a \$\text{Mo}/n^+\text{-GaAs}\$ Schottky contact for nano-scale III-V MOSFETs](#)

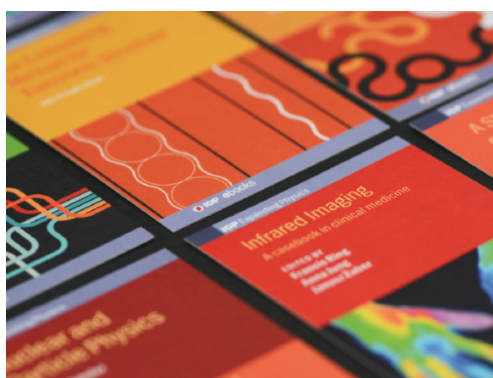
M Aldegunde, S P Hepplestone, P V Sushko *et al.*

- [Partitioned densities of states in a resonant tunnelling structure](#)

Xuean Zhao

- [Atomic structures and electronic properties of Ni or N modified Cu/diamond interface](#)

Xue-Rong Shi, Simin Huang, Yue Huang *et al.*



IOP | ebooks™

Bringing together innovative digital publishing with leading authors from the global scientific community.

Start exploring the collection—download the first chapter of every title for free.

Resonant inelastic soft x-ray scattering on LaPt₂Si₂

Deepak John Mukkattukavil^{1,*} , Johan Hellsvik^{2,3} , Anirudha Ghosh⁴,
Evanthia Chatzigeorgiou¹ , Elisabetta Nocerino⁵, Qisi Wang⁶ , Karin von Arx^{6,9} ,
Shih-Wen Huang⁴ , Victor Ekholm⁴ , Zakir Hossain⁷, Arumugum Thamizhavel⁸ ,
Johan Chang⁶ , Martin Månsson⁵ , Lars Nordström¹ , Conny Sâthe⁴ ,
Marcus Agåker^{1,4} , Jan-Erik Rubensson¹  and Yasmine Sassa^{9,*} 

¹ Department of Physics and Astronomy, Uppsala University, Box 516, SE-751 20 Uppsala, Sweden

² PDC Center for High Performance Computing, KTH Royal Institute of Technology, SE-106 91 Stockholm, Sweden

³ Nordita, KTH Royal Institute of Technology and Stockholm University, Hannes Alfvéns väg 12, SE-106 91 Stockholm, Sweden

⁴ MAX IV Laboratory, Lund University, SE-221 00 Lund, Sweden

⁵ Department of Applied Physics, KTH Royal Institute of Technology, SE-106 91 Stockholm, Sweden

⁶ Physik-Institut, Universität Zürich, Winterthurerstrasse 190, CH-8057 Zürich, Switzerland

⁷ Department of Physics, Indian Institute of Technology, Kanpur 208016, India

⁸ DCMFMS, Tata Institute of Fundamental Research, Mumbai 400005, India

⁹ Department of Physics, Chalmers University of Technology, Göteborg, SE-412 96, Sweden

E-mail: deepak.john_mukkattukavil@physics.uu.se and yasmine.sassa@chalmers.se

Received 31 January 2022, revised 3 May 2022

Accepted for publication 31 May 2022

Published 15 June 2022



Abstract

X-ray absorption and resonant inelastic x-ray scattering spectra of LaPt₂Si₂ single crystal at the Si 2*p* and La 4*d* edges are presented. The data are interpreted in terms of density functional theory, showing that the Si spectra can be described in terms of Si *s* and *d* local partial density of states (LPDOS), and the La spectra are due to quasi-atomic local 4*f* excitations. Calculations show that Pt *d*-LPDOS dominates the occupied states, and a sharp localized La *f* state is found in the unoccupied states, in line with the observations.

Keywords: resonant inelastic x-ray scattering, superconductivity, charge density wave, local partial density of states

(Some figures may appear in colour only in the online journal)

1. Introduction

In the last two decades, resonant inelastic x-ray scattering (RIXS) has played an essential role in the understanding of many-body physics. By probing the change of energy,

momentum, and polarization of the scattered photon, the RIXS technique provides access and information to intrinsic excitations in complex materials [1]. In the latest years, the drastic improvement of the technique has pushed forward the study of systems combining superconductivity (SC) and charge- and/or spin-density waves (CDW and/or SDW). Materials like Fe/Ni-based pnictides [2, 3], transition metal dichalcogenides [4, 5], or cuprate superconductors [6–13] are three examples out of many.

Recently, the quasi-two-dimensional Pt-based rare earth intermetallic material LaPt₂Si₂ has attracted a lot of attention as it exhibits strong interplay between CDW and SC [14].

* Authors to whom any correspondence should be addressed.



Original Content from this work may be used under the terms of the [Creative Commons Attribution 4.0 licence](https://creativecommons.org/licenses/by/4.0/). Any further distribution of this work must maintain attribution to the author(s) and the title of the work, journal citation and DOI.

A first order transition was reported from high-temperature tetragonal to low-temperature orthorhombic phase, accompanied by a CDW transition around $T_{\text{CDW}} = 112$ K followed by a SC transition at $T_c = 1.22$ K. LaPt_2Si_2 crystallizes in a CaBe_2Ge_2 -type tetragonal structure (space group $P4/nmm$, see figure 1(a)), having a resemblance to the ThCr_2Si_2 -type structure found in pnictide and heavy fermion systems. The structure also has close resemblance to the 122 superconducting Fe based systems, where spin fluctuations have been investigated and debated [2, 15, 16]. The striking difference between these two structures is that the former one lacks inversion symmetry in the crystal, resulting in two non-equivalent layers ($\text{Si}_1\text{-Pt}_1\text{-Si}_1$) and ($\text{Si}_2\text{-Pt}_2\text{-Si}_2$) arranged in alternating stacking separated by La atoms [17] (as shown in figure 1(a)). This special feature in the crystal structure is reminiscent of noncentrosymmetric SC [14], where the lack of inversion symmetry results in nonuniform lattice potential, creating an asymmetric spin-orbit coupling (SOC).

To understand the material, we have performed x-ray absorption (XAS) and RIXS experiments on a LaPt_2Si_2 single crystal at the Si $2p$ ($L_{2,3}$) and La $4d$ ($N_{4,5}$) edges at room temperature, above the CDW and SC states. To the best of our knowledge, XAS and RIXS measurements have not been reported on this compound so far, and this preliminary study focuses on understanding the features observed above the SC and CDW transitions and how they relate to theoretical models and previous reports of XAS and RIXS from La and Si-based compounds. A review on methods for theoretical modeling on RIXS spectra can be found in [18], and effects of self-interacting interaction beyond standard density functional theory (DFT) are treated in [19].

The XAS spectrum shows sharp peaks at 97.1 eV, 101.47 eV and a dominating broad feature with maximum at 117.4 eV which can be assigned to excitation of atomic-like La $4d^{-1}4f$ states. RIXS spectra excited at these resonances show scattering to La $5p^{-1}4f$ final states, and we also observe x-ray emission (XES) from the dynamically populated $4d^{-1}4f^3D_1$ state to the ground state. The Si XES spectrum is stationary on the emission energy scale, and partial fluorescence yield (PFY) is used to construct the Si $2p$ XAS spectrum. Using DFT we show that the Si XES spectra can be described in terms of Si s and d local partial density of states (LPDOS). While Pt d -LPDOS is predicted to dominate the occupied states, a sharp localized La f state is found in the unoccupied states, in line with the observed quasi-atomic excitations. XAS and RIXS measurements show that the material's basic interactions can be explained using LPDOS of Si.

2. Experiment

The single crystalline sample of LaPt_2Si_2 used in this study was synthesized using the Czochralski pulling method [14]. Crystallographic analysis shows that the LaPt_2Si_2 sample has $P4/nmm$ space group with the crystallographic parameters given in figure 1(a). The VESTA software [20] was used to generate the crystal structure with crystallographic parameters from Gupta *et al* [14]. The size of the sample used in this

study was $\approx 1 \text{ mm} \times 2 \text{ mm}$ (figure 1(b)). A diffraction pattern, obtained at room temperature using the Laue backscattering method (figure 1(c)) shows that the sample is a single crystal.

XAS and RIXS spectra were measured at the SPECIES beamline [21, 22] at MAX IV Laboratory in Lund, Sweden. A Si wafer was attached to the sample holder for the beamline monochromator energy calibration (figure 1(b)). Total electron yield (TEY) was measured via the drain current, both on the LaPt_2Si_2 sample, and the Si wafer. Normalization of TEY with respect to beamline flux was achieved via the gold-coated refocusing mirror drain current. The TEY measured from the Si wafer was in good agreement with previous Si $L_{2,3}$ edge XAS measurements [23].

XES spectra were measured using the Scientia model XES-350 spectrometer [24], which is a Rowland spectrometer equipped with three gratings and a micro-channel plate-based delay line detector [25]. For the measurements reported in this article, a grating with 3 m radius and 300 l mm^{-1} groove density was used. Energy calibration of the spectrometer relative to the monochromator was done using the elastic scattering of the incident photon beam, and the monochromator energy scale was set by the Si $L_{2,3}$ XAS [23]. The overall resolution was estimated from the full width at half maximum (FWHM) of the elastic scattering peak to be 270 meV at 108 eV incident photon energy. All RIXS measurements were carried out in the horizontal plane at 90° scattering angle, and to minimize diffuse elastic scattering the incident radiation was linearly polarized in the horizontal direction.

3. Theory

DFT calculations of the electronic structure of LaPt_2Si_2 have been performed with the Elk code [26] which implements the full-potential augmented plane waves and local orbitals method (FP-APW+lo) [27]. The core electrons are modeled with four component wave functions, and the valence electron are modeled with two-component wave functions, augmented optionally with SOC in (l, s) basis. In tetragonal LaPt_2Si_2 structure, the primitive cell contains ten atoms. Calculations have been performed for this structure, using the lattice parameters reported by Gupta *et al* [17]. We used the generalized gradient approximation as parameterized in the Perdew–Burke–Ernzerhof (PBE) functional [28] for non-magnetic, collinear spin-polarized, and noncollinear magnetic including SOC calculations, using a maximum angular momentum $l=8$, and a Γ -centered k -point mesh of size $16 \times 16 \times 16$.

In order to consider whether to go beyond DFT to treat the atomic-like localized La $4f$ electrons, we make the observation that in the PBE-DFT calculations (shown in figure 3) there are no occupied La $4f$ states, as these reside about 2 eV above the Fermi level. By construction a self-interaction calculation would not change things as the La $4f$ state are not occupied. Similarly, DFT+U treatment of these states would not change the electronic structure. Therefore we have chosen not to go beyond DFT for calculating the electronic structure. As both highly localized and highly delocalized states contribute to the

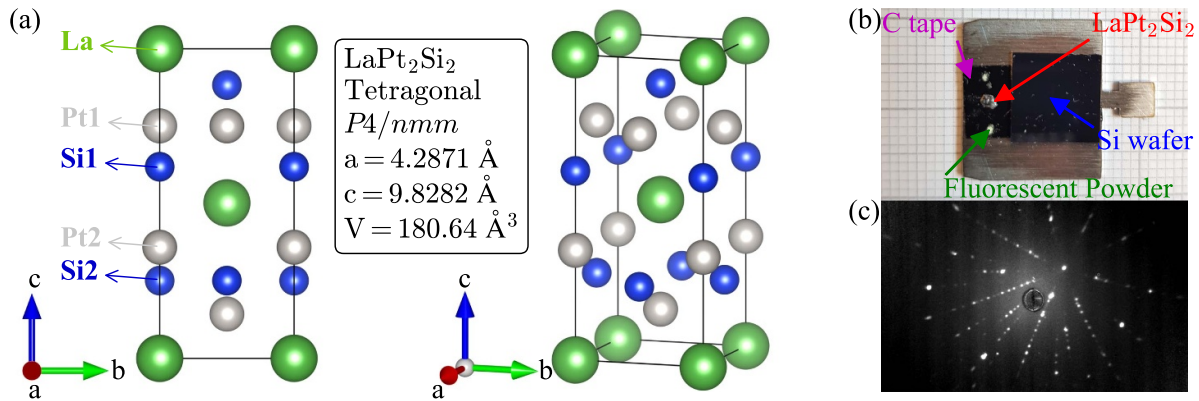


Figure 1. (a) Crystal structure of LaPt_2Si_2 viewed in two different directions, lattice parameters, and different crystallographic sites of Si and Pt. (b) LaPt_2Si_2 crystal mounted on sample plate. Conductive carbon tape was used as adhesive, fluorescence powder for spotting beam, and a Si wafer was used for calibrating the beamline energy. (c) The Laue diffraction pattern demonstrates the crystallinity of the sample.

spectra no attempts were made to explicitly capture the excitations, e.g. by constructing a model Hamiltonian based on the ground-state DFT result.

4. Results and discussion

In the Elk PBE collinear spin-polarized calculation, the electron band structures for majority and minority spins comes out as degenerate, from which we infer that LaPt_2Si_2 is a non-magnetic material. The electronic band structure in Elk PBE SOC calculation is shown in figure 2, with the associated total DOS, and projected partial DOS for different crystallographic sites La, Pt₁, Si₁, Pt₂ and Si₂ are shown in figure 3. At the La site a sharp La *f*-LPDOS peak dominates the unoccupied states, and two sharp peaks in the La *p*-LPDOS are found below -15 eV in the occupied states (figure 3(a)). It can be concluded that the La states are localized and do not contribute much to the band formation. The occupied states are dominated by Pt *d*-LPDOS with a maximum around -4 eV (figures 3(b) and (e)) whereas *p*-symmetry gives the largest contribution to the electronic structure at the Si sites (figures 3(c) and (f)), apart from a sharp peak in the Si *s*-LPDOS at around -10 eV. By virtue of the dipole selection rules, x-ray spectra at the Si $L_{2,3}$ edges primarily probe the Si (*s* + *d*)-LPDOS, and reflect the localized nature of the La *f*-excitations at the La $4d$ edges.

Figure 4(a) shows TEY obtained by the drain current from LaPt_2Si_2 as a function of incident photon energy. There are two sharp peaks at 97.1 eV and 101.47 eV, and a dominating broad feature with maximum at 117.4 eV, which can be assigned to excitation of atomic-like La $4d^{-1}4f$ states, including transitions to the bound LS-forbidden 3P_1 and 3D_1 states, and the giant 1P_1 resonance, respectively. Similar multiplet structures are typically observed in La compounds [29–32], as a consequence of the atomic-like localized nature of the $4f$ electrons. Notably, the TEY spectrum does not capture the Si $2p$ edge XAS of LaPt_2Si_2 , expected to appear just below 100 eV. This observation demonstrates that the La $4d$ absorption cross-section totally dominates over Si $2p$ absorption. Instead, we observe TEY peaks between 104 and 108 eV

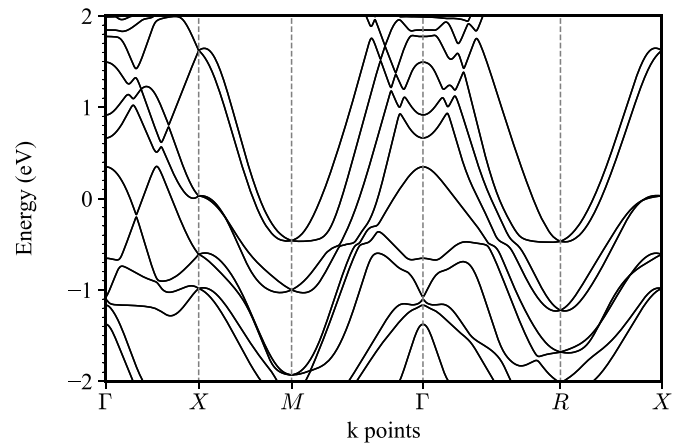


Figure 2. Electronic band structure in Elk PBE SOC calculation along different reciprocal lattice directions. Nearly degenerate bands are split by the SOC.

(figure 4(a)) that match previous XAS spectra of SiO_2 [23]. We attribute these peaks to an oxide layer formed on the surface of LaPt_2Si_2 crystal.

To address the Si $2p$ edge absorption spectrum of LaPt_2Si_2 we first turn our attention to the XES map in figure 4(d). A complex pattern is observed, where the main intensity is stationary between 87 eV and 98 eV emission energy, primarily changing its integrated intensity with excitation energy. There is also an elastic peak for which the emission energy equals the excitation energy. A weaker structure disperses at constant 20–24 eV energy loss, and a sharp emission feature is observed at 101.46 eV constant emission energy. The latter is resonantly excited at incident photon energies around 120 eV. These features are denoted in the XES spectrum excited at 129.8 eV, shown in figure 4(c) as:

- (i) Elastic scattering, coinciding with the incident photon energy.
- (ii) A constant energy loss feature which we assign to the scattering to $5p^{-1}4f$ final states, reached over the $4d^{-1}4f$ resonances. We tentatively assign the two peaks at 20.8 and

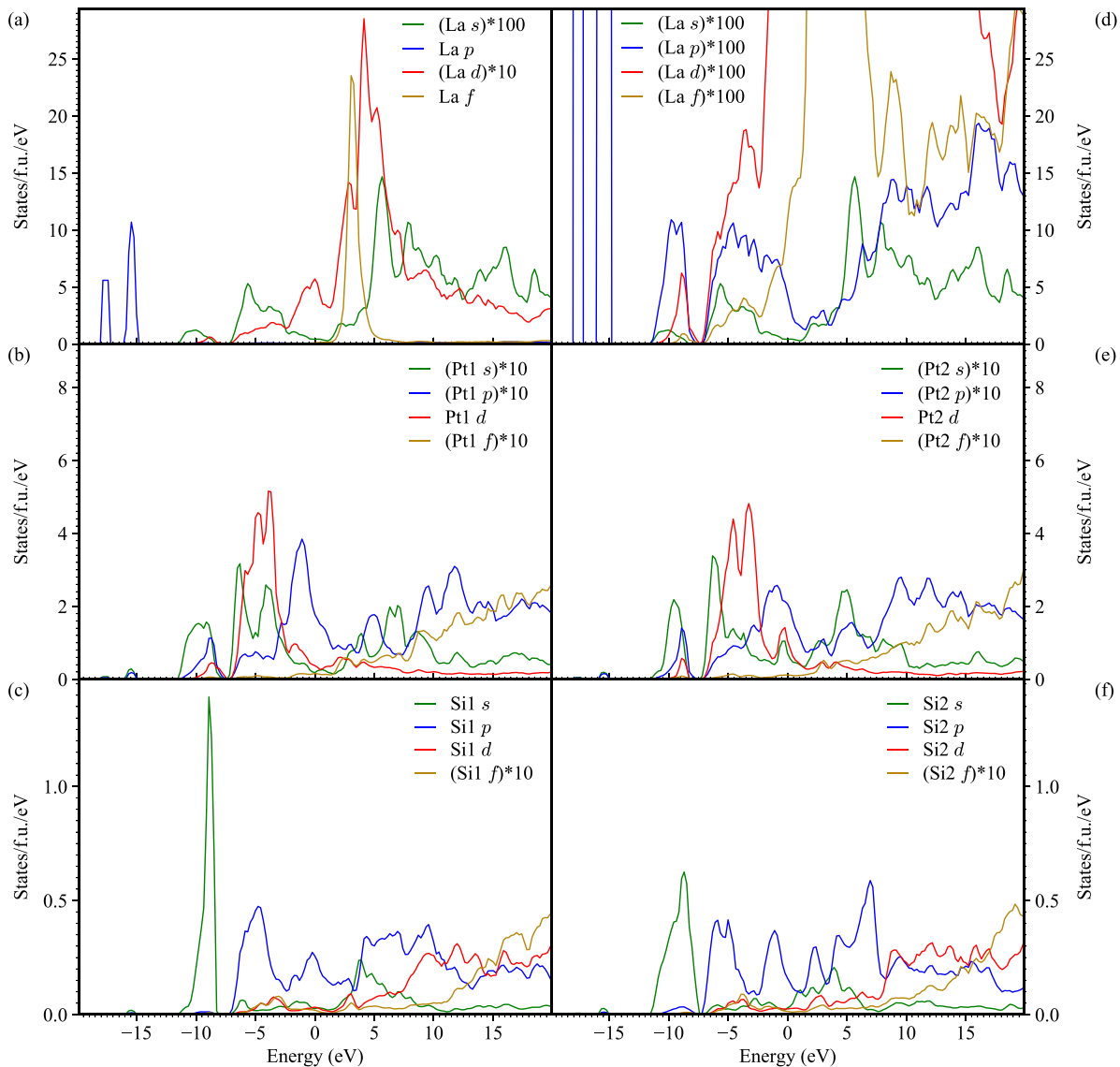


Figure 3. Partial electronic DOS in Elk PBE SOC calculation for (a) La, (b) Pt₁, and (c) Si₁ crystallographic sites in left panel and (d) La (multiplied by 100 to show the possible hybridization of La *p* and *d* states with Pt and Si), (e) Pt₂, and (f) Si₂ in right panel. In order to accommodate the data in the panels, some of the components have been multiplied with a factor of 10 or 100.

22.5 eV energy loss to final triplet states and the ¹D₂ state, respectively, following the analysis of Suljoti *et al* [32] and Miyahara *et al* [33].

- (iii) A sharp peak at 101.46 eV emission energy assigned to emission from the dynamically excited 4d⁻¹4f³D₁ state to the La 4f⁰ ground state.
- (iv) A broad feature at constant emission energy, which we assign to principally Si L_{2,3} emission, i.e. is associated with electrons from the valence band filling Si 2*p* vacancies.
- (v) Si L_{2,3} emission as in (iv), but as we see, the excitation energy dependence of the two features are different.

The magenta curve in figures 4(a) and (b) is the PFY, constructed to emphasize Si 2*p* excitations. As Si L_{2,3} emission dominates features (iv) and (v), intensity in the corresponding 85–98 eV emission energy range was integrated to construct

the PFY spectrum, while intensity from the dispersing La feature (ii), which contributes in the 110–120 eV excitation-energy range (figure 4(c) inset) was subtracted. The Si L_{2,3} edge shown in the PFY spectrum is found at 99.5 eV, and there is a sharp second intensity increase at 101.4 eV, almost coinciding with the La ³D₁ resonance, and another intensity increase around 107 eV.

There is only a faint (<10%) structure in PFY at the sharp SiO₂ excitations around 104 eV which can be attributed to the surface oxide. For oxidized Si surfaces, a similar observation has been made for oxide layers of around 7 nm thickness [23]. While the fluorescence yield sampling depth in Si is estimated to be 70 nm [23], it is similar in this compound except for the region of the La giant resonance ¹P₁ where the sampling depth is more than three-fold reduced [34]. We can therefore estimate the oxide layer also for LaPt₂Si₂ to be in the ≈7 nm range.

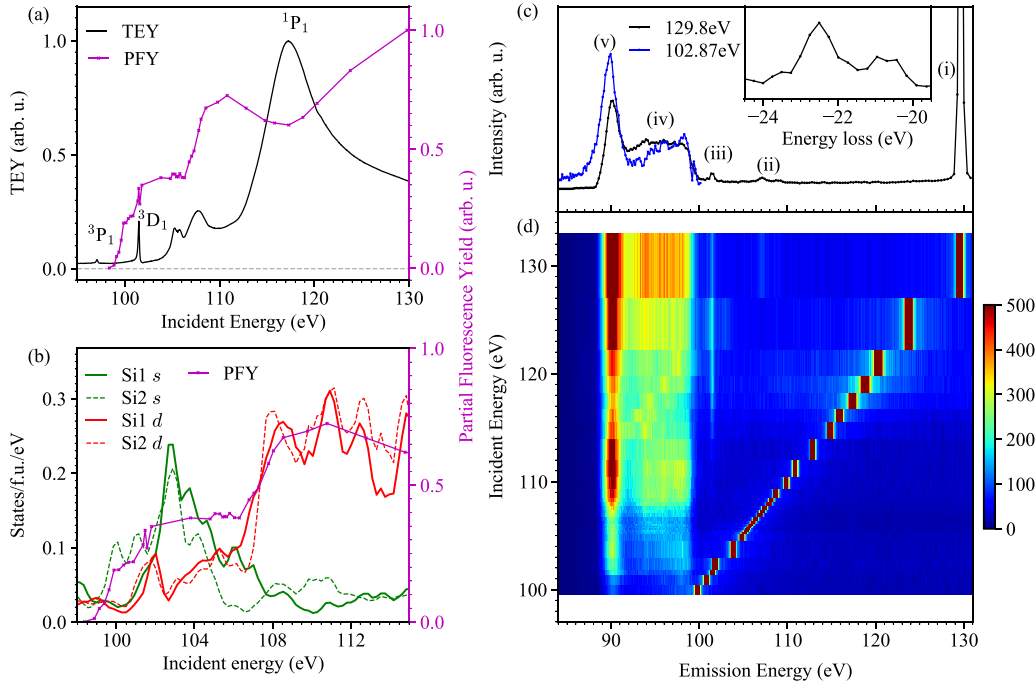


Figure 4. (a) TEY (black) measured using drain current from sample and PFY (magenta) for emission in the 85–98 eV range, with the dispersing feature (ii) subtracted. (b) Zoomed-in PFY for emission in the 85–98 eV range (magenta) with DOS of Si₁ *s* (green), Si₂ *s* (dash green), Si₁ *d* (red), Si₂ *d* (dash red) above Fermi energy. (c) An overview XES spectrum from LaPt₂Si₂ at incident photon energy of 129.8 eV, covering emission energies up to 130 eV (black). In the corresponding detector position, the low-energy part of the spectrum is not fully covered. The spectrum showing the full low-energy range is measured in a separate measurement at 102.87 eV excitation energy (blue). The two spectra are normalized in the 95–100 eV range. The emission features are denoted: (i) elastic peak, (ii) resonant scattering to La 5*p*⁻¹4*f* final states, which is also shown in the inset on the energy-loss scale, (iii) emission from the dynamically populated La 4*d*⁻¹4*f* ³D₁ state, and (iv), (v) stationary feature primarily associated with Si L_{2,3} emission. (d) XES map. Like in the overview spectrum in panel (c) the attenuation of the XES emission at the lowest energies is an experimental artifact due to the drop in sensitivity at this detector position.

While the Si L_{2,3} edge PFY spectrum gives information about the bulk material below the surface oxide layer, it does not directly represent the cross-section for Si 2*p* excitations. The PFY minimum at 117.3 eV coincides with the maximum of the La giant resonance. At these energies, La 4*d* absorption dominates the XAS spectrum of LaPt₂Si₂. As this process competes with Si 2*p* absorption, and since La 4*d* holes do not emit appreciably in the chosen emission energy range, the observed broad dip in the PFY is expected. The mechanism is the same as exploited in the inverse partial yield method [35].

In figure 4(b) we compare the the PFY with the Si *s* and *d* LPDOS, separated into contributions from the Si₁ and Si₂ sites. Significant differences between the two sites are predicted, e.g. the absorption close to the edge is primarily of Si₂ *s* character. The PFY increase around 101.4 eV coincides with increasing Si₁ *s*-LPDOS, while the 107 eV increase matches the increase in the combined Si *d*-LPDOS. We assign the main PFY features accordingly.

4.1. Elastic peak (i)

In general, the elastic peak (i) can have contributions from both diffuse reflection and the resonant absorption-emission process. Emission from the giant resonance in La compounds in low-energy electron excited spectra seemingly coincides

with the absorption [29], demonstrating that a captured electron is sufficiently localized to recombine with the 4*d* hole. The giant resonance is also observed in x-ray reflection measurements [30]. Considering the complex index of refraction, $n + ik$, it has been noted that if $(n - 1)^2 \ll k^2 \ll (n + 1)^2$ the normal incidence reflectivity varies as the square of the absorption cross section. While this is often the case in this energy range [36], this approximation does not hold at the giant resonance, for which tabulated optical constants [34] imply a high-energy shift of the reflectivity peak relative to the peak in the absorption cross section. This predicted shift is consistent with the observed difference in peak positions when comparing the excitation-energy dependence of the elastic peak intensity and the TEY spectrum (figure 5). While the curves show similarities, there are also significant differences, the TEY spectrum peaks at 117.5 eV, and the maximum in the elastic-peak intensity is around 119 eV. Although we note that the TEY signal may be influenced by disorder in the topmost layers of the crystal, we can conclude that the elastic peak is dominated by diffuse reflection in the region of the giant resonance.

4.2. Dispersing feature (ii)

The dispersing double-peak feature (ii), assigned to La ground state $\rightarrow 4d^{-1}4f \rightarrow 5p^{-1}4f$ scattering is shown in the inset of figure 4(c). The two peaks are fitted with Gaussian

at 22.5 eV and 20.7 eV energy loss, with FWHM of 1.1 eV and 1.0 eV, respectively. The energy positions are close to the corresponding transitions in ionic La compounds [31, 32], facilitating the assignment of the high-energy loss peak to the 1D_2 final state, and the low-energy loss peak to ‘spin-flip’ 3D_J states. The intensity ratio of the two peaks also coincides with the earlier studies, again demonstrating the atomic-like nature of the scattering at the La sites.

In the ionic compounds the $5p^{-1}4f$ final states are situated in the band gap, whereas in the present case they are found in the conduction band far above the $5p^{-1}$ ionization thresholds. Therefore, delocalization via interaction with the continuum is allowed, just like in the case of the giant $4d^{-1}4f^1P_1$ resonance. We tentatively attribute the additional width to tunneling of the excited electron through a barrier, analogously to the case of the singlet $4d^{-1}4f$ state. With this interpretation the increased width implies a reduction of the lifetime of the $5p^{-1}4f$ final states to less than one femtosecond due to this additional decay channel.

4.3. Emission at 101.46 eV (iii)

Within the measurement accuracy, the energy of the stationary feature (iii) (figure 4(c)), $101.46 (\pm 0.09)$ eV, matches the energy of the La $4d^{-1}4f^3D_1$ resonance (101.47 eV). Therefore, it can be assigned to transitions from this 3D_1 state to the La ground state. The mechanism for off-resonance population of $4d^{-1}4f$ states in La compounds has been addressed earlier [29, 30], and the associated population of La $3d^{-1}4f$ states have been termed ‘shake-down’ [37]. The transition energy is below the $4d$ binding energies [38], i.e. the $4d$ hole pulls down the $4f$ orbitals below threshold. Consequently, the $4d$ holes are screened as an electron from the valence band fills the $4f$ level, forming $4d^{-1}4fV^{-1}$ states, where V^{-1} denotes a hole in the valence band. If this hole in the valence band delocalizes prior to the decay, the transition mirrors the 3D_1 resonance.

In figure 5 we see that the intensity of the 3D_1 emission to a large extent follows the absorption cross section, which is in line with the notion that the cross section in the range is totally dominated by La $4d$ excitations. However we find the maximum in the 3D_1 yield slightly above 120 eV, and more than 2.5 eV above the absorption maximum. This shift can be understood by considering the delocalization of the initially excited electron. It is well-known that the probability that this electron tunnels through the potential barrier prior to the core hole decay increases with excitation energy over the giant resonance [31, 39]. As long as the initial electron remains local it contributes to the screening of the $4d$ hole and hampers alternative screening mechanisms. Only when it delocalizes the screening from the valence band to the triplet coupled $4d^{-1}4fV^{-1}$ states becomes important. In this way the 3D_1 yield in this range reflects a dynamical process where the $4d^{-1}4f^1P_1$ excitation is followed by tunneling of the $4f$ electron, and subsequent screening from the valence band to triplet coupled $4d^{-1}4fV^{-1}$ states. In this sense the 3D_1 yield monitors the cross section for excitation of unscreened La $4d$ holes.

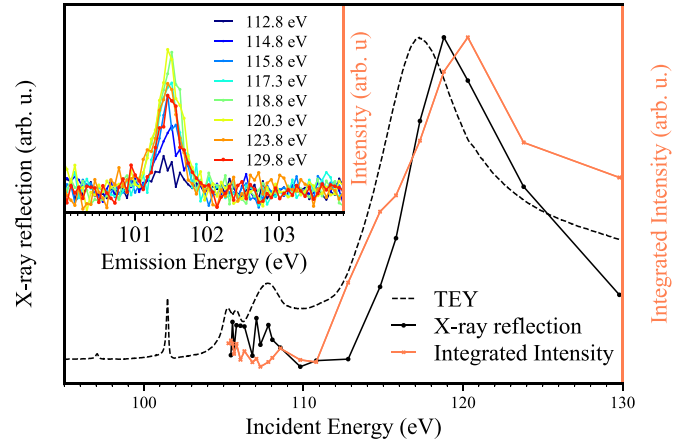


Figure 5. Elastic peak (i) intensity, dominated by diffuse x-ray reflectivity (dotted black), and intensity of the stationary feature ((iii) see inset), associated with La $4d^{-1}4f^3D_1 \rightarrow 4f^0$ transition (dotted coral) compared to the TEY spectrum (dashed black).

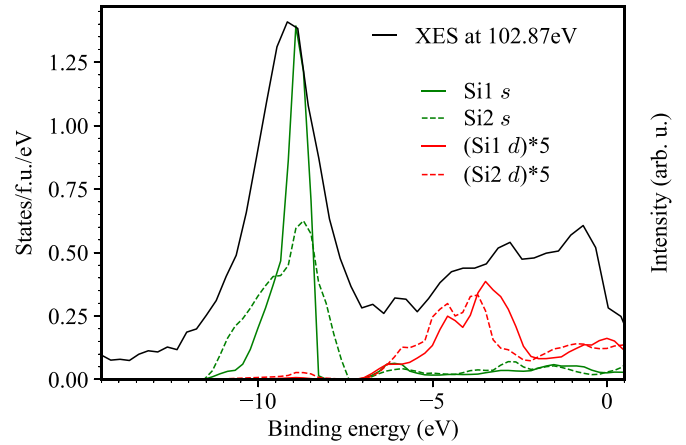


Figure 6. XES spectrum excited at 102.87 eV, shifted to the binding energy scale by subtracting 98.7 eV (black) is compared to the Si1 s (green) and Si2 s (dashed green) LPDOS, and the Si1 d (red) and Si2 d (dashed red) LPDOS, below the Fermi level.

4.4. Si 2p emission (iv and v)

4.4.1. LPDOS and XES. The XES spectrum shown in figure 6, excited at 102.87 eV, is shifted to the binding energy scale by subtracting 98.97 eV, as determined by the apparent valence band edge. From the edge, the spectrum shows a plateau down to around -6 eV, followed by a peak with a maximum around -9.5 eV. The experimental results are compared to the Si s and d LPDOS (figure 6) at the two crystallographic sites, Si₁ and Si₂, as denoted in figure 1(a). The low-energy peak can be unambiguously assigned to transitions from states of Si s character as the Si s -LPDOS dominates in this region. In the predicted LPDOS there is a marked difference between the two sites. Whereas the Si₁ s -LPDOS has a rather sharp peak at -9 eV, the Si₂ s -LPDOS is more smeared out. Due to the broadening mechanisms, especially the lifetime broadening of final hole states far from the Fermi level [40] we do not expect this difference to be observable.

The Si s -LPDOS is not sufficient to capture the plateau in XES spectrum between the valence band edge and -6 eV, as density relative to the -9 eV peak is small in this region. Assuming that the Si d -LPDOS gives a factor of five larger contribution to the XES intensity than the Si s -LPDOS, the intensity in this region can be partly explained (figure 6). Since the Si $2p$ - d radial overlap typically is larger than the $2p$ - s overlap, Si d -states are expected to contribute more to Si $2p$ emission than Si s -states [41], but a factor of five is unusually large. We also note that upscaled Si d -LPDOS introduces spectral structure that is not observed in the experimental spectrum.

4.4.2. Excitation-energy dependence. The spectral changes as the excitation energy varies across the La 3D_1 absorption peak are shown in figure 7. We find that the spectra normalized at 98 eV, show a steep resonant behavior where the intensity of the peak at 90 eV (-9 eV peak in figure 6) increases, and a pronounced shoulder develops around 91 eV, and attains maximum intensity when the incident energy is tuned to the La 3D_1 resonance.

It is tempting to interpret this behavior as due to transitions involving La $4d^{-1}4f^3D_1$ intermediate state. In this state the f electron is localized at the La site, and in principle a valence electron can fill the core hole, to create a final state with a vacancy in the valence band and an excited f electron. The sharp peak in the unoccupied La f -LPDOS of the electronic ground state (figure 3(a)) suggests that the f electron is localized also in the final state. According to dipole selection rules transitions from the valence band to a La $4d$ hole should be from state with La p or f character. However, the theory does not show appreciable LPDOS of these local symmetries (figure 3(a)), and it lacks steep structures that could directly account for the observations.

Tentatively, we still associate the resonant behavior to transitions to the La $4d$ level from the valence band. With the excitation energy at 101.47 eV, and the emission energy of the resonant shoulder is 91 eV, the energy loss is 10.5 eV, suggesting that the corresponding hole is in the band that is dominated by Si s states. Especially, the Si₁ site, which is in closest proximity to the La atoms (figure 1(a)) has a sharp peak at the corresponding energy (figure 3(c)). The observations are consistent with a ‘cross transition’ where the final state has an electron in the band dominated by La f -LPDOS or La p -LPDOS (figure 3(d)) and a vacancy in the band dominated by Si₁ s -LPDOS, and we speculate that excitonic effects, and possibly interference between close lying core hole states may enable pathways to such final states. Finally we note that there is a slight spectral change, when comparing data taken below and above the resonance. They are consistent with selective excitation of the two Si sites, which show large variation at the cross section at these excitation energies (figure 4(b)).

This possible hybridization effects of La with the close Si₁ site might be a key to understanding the predictions put forth in theoretical calculations by Kim *et al* [42] where the CDW is predicted to be confined to the layer with Pt₁ crystallographic site. We speculate that by understanding these local excitations of La with the Si₁ atoms could indicate

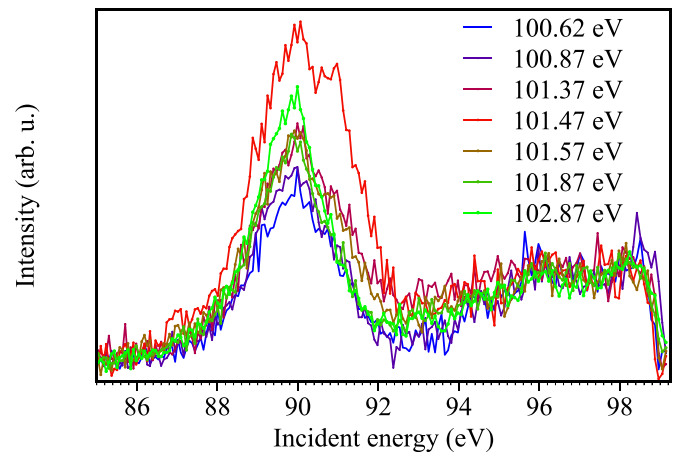


Figure 7. XES spectra normalized at 98 eV, excited in the region of La $4d^{-1}4f^3D_1$ resonance.

how hybridization might aid or prevent the formation of multiple CDW, which are observed in recent experiments [43]. The La atoms are not merely spectators that separate the Si₁-Pt₁-Si₁ and Si₂-Pt₂-Si₂ layers but might play a crucial role in the formation of CDW in LaPt₂Si₂.

5. Conclusions

XAS and RIXS measurements at Si $2p$ and La $4d$ edges of LaPt₂Si₂ are presented, and interpreted in terms of DFT calculations. Atomic-like local La $4d \rightarrow 4f$ excitations are found in the absorption spectrum, the LS-forbidden 3P_1 , and 3D_1 excitation as well as the giant 1P_1 resonance. Decay to $5p^{-1}4f$ final states are observed, and also the decay of the dynamically populated 3D_1 state to the electronic ground state. Observations suggest that resonantly excited 3D_1 states also decay via valence band emission. The Si $2p$ XAS spectra are measured via PFY, and the XES spectra are independent of the excitation energy over most of the energy range. The spectra are assigned using the theoretical LPDOS of Si s and d character at both crystallographic Si sites. We should expect to see a variation in electronic interaction between La and Si atoms as a function of temperature, and an accompanying variation in the Si $2p$ and La $4d$ spectra. With site selectivity the question to what extent the CDW primarily is formed in the Si₁-Pt₁-Si₁ or Si₂-Pt₂-Si₂ layers can be addressed. A more detailed study will follow, including a systematic investigation of the temperature dependence across the CDW transition, and the dependence on crystal orientation.

Data availability statement


All data that support the findings of this study are included within the article (and any supplementary files).

Acknowledgments

The authors would like to thank Margit Andersson and Jenn-Min Lee for the technical support during the experiments

at SPECIES beamline at MAX IV. Y S acknowledges funding from the Area of Advance - Material Sciences from the Chalmers University of Technology and the Swedish Research Council (VR) Starting Grant (Dnr. 2017-05078). M M and E N acknowledge funding from the Swedish Research Council (VR) through a neutron project Grant (Dnr. 2016-06955), the Swedish Foundation for Strategic Research (SSF) within the Swedish national graduate school in neutron scattering (SwedNess), and the Carl Tryggers Foundation for Scientific Research (CTS-18:272). M A acknowledges funding from Stiftelsen for Strategisk Forskning (SSF), through grant RIF14-0064. J-E R acknowledges funding from the Swedish Research Council (VR) and the Carl Tryggers Foundation (CTS). The computations were enabled by resources provided by the Swedish National Infrastructure for Computing (SNIC) at PDC and NSC, partially funded by the Swedish Research Council through Grant Agreement No. 2018-0597.

ORCID iDs

Deepak John Mukkattukavil  <https://orcid.org/0000-0003-1311-7358>

Johan Hellsvik  <https://orcid.org/0000-0003-0210-4340>

Evanthia Chatzigeorgiou  <https://orcid.org/0000-0001-5183-8020>

Qisi Wang  <https://orcid.org/0000-0002-8741-7559>

Karin von Arx  <https://orcid.org/0000-0002-8367-5454>

Shih-Wen Huang  <https://orcid.org/0000-0003-0349-4125>

Victor Ekholm  <https://orcid.org/0000-0002-3797-3346>

Arumugum Thamizhavel  <https://orcid.org/0000-0003-1679-4370>

Johan Chang  <https://orcid.org/0000-0002-4655-1516>

Martin Månsson  <https://orcid.org/0000-0002-3086-9642>

Lars Nordström  <https://orcid.org/0000-0002-1400-2336>

Conny Sâthe  <https://orcid.org/0000-0001-7799-8575>

Marcus Agåker  <https://orcid.org/0000-0001-6501-5324>

Jan-Erik Rubensson  <https://orcid.org/0000-0003-1467-8114>

Yasmine Sassa  <https://orcid.org/0000-0003-1416-5642>

References

- [1] Ament L J P, van Veenendaal M, Devereaux T P, Hill J P and van den Brink J 2011 *Rev. Mod. Phys.* **83** 705–67
- [2] Fernandes R M, Coldea A I, Ding H, Fisher I R, Hirschfeld P J and Kotliar G 2022 *Nature* **601** 35–44
- [3] Lumsden M D and Christianson A D 2010 *J. Phys.: Condens. Matter* **22** 203203
- [4] Xu Z et al 2021 *Nanotechnology* **32** 492001
- [5] Manzeli S, Ovchinnikov D, Pasquier D, Yazyev O V and Kis A 2017 *Nat. Rev. Mater.* **2** 17033
- [6] Wang Q et al 2020 *Phys. Rev. Lett.* **124** 187002
- [7] Wang Q et al 2021 *Sci. Adv.* **7** eabg7394
- [8] Wang Q et al 2022 *Nat. Commun.* **13** 1795
- [9] Gupta N K et al 2021 *Proc. Natl Acad. Sci.* **118** e2106881118
- [10] Tranquada J M, Dean M P M and Li Q 2021 *J. Phys. Soc. Japan* **90** 111002
- [11] Arpaia R and Ghiringhelli G 2021 *J. Phys. Soc. Japan* **90** 111005
- [12] Imada M 2021 *J. Phys. Soc. Japan* **90** 111009
- [13] Keimer B, Kivelson S A, Norman M R, Uchida S and Zaanen J 2015 *Nature* **518** 179–86
- [14] Gupta R, Dhar S K, Thamizhavel A, Rajeev K P and Hossain Z 2017 *J. Phys.: Condens. Matter* **29** 255601
- [15] Li Y et al 2019 *Phys. Rev. Lett.* **122** 117204
- [16] Chen J, Gamza M B, Banda J, Murphy K, Tarrant J, Brando M and Grosche F M 2020 *Phys. Rev. Lett.* **125** 237002
- [17] Gupta R, Paramanik U B, Ramakrishnan S, Rajeev K P and Hossain Z 2016 *J. Phys.: Condens. Matter* **28** 195702
- [18] van den Brink J 2016 Resonant inelastic x-ray scattering on elementary excitations *Quantum Materials: Experiments and Theory, Modeling and Simulation* vol **6**, 1st edn, ed E Pavarini, E Koch, J van den Brink and G Sawatzky (Jülich: Forschungszentrum) ch 12
- [19] Arola E, Horne M, Strange P, Winter H, Szotek Z and Temmerman W M 2004 *Phys. Rev. B* **70** 235127
- [20] Momma K and Izumi F 2011 *J. Appl. Crystallogr.* **44** 1272–6
- [21] Urpelainen S et al 2017 *J. Synchrotron Radiat.* **24** 344–53
- [22] Kokkonen E et al 2021 *J. Synchrotron Radiat.* **28** 588–601
- [23] Kasrai M, Lennard W N, Brunner R W, Bancroft G M, Bardwell J A and Tan K H 1996 *Appl. Surf. Sci.* **99** 303–12
- [24] Nordgren J and Guo J 2000 *J. Electron Spectrosc. Relat. Phenom.* **110–111** 1–13
- [25] Oelsner A, Schmidt O, Schicketanz M, Klais M, Schönhense G, Mergel V, Jagutzki O and Schmidt-Böcking H 2001 *Rev. Sci. Instrum.* **72** 3968–74
- [26] The Elk code (available at: <http://elk.sourceforge.net/>)
- [27] Singh D J and Nordström L 2006 *Planewaves, Pseudopotentials and the LAPW Method* 2nd edn (Boston, MA: Springer)
- [28] Perdew J P, Burke K and Ernzerhof M 1996 *Phys. Rev. Lett.* **77** 3865–8
- [29] Ichikawa K, Nisawa A and Tsutsumi K 1986 *Phys. Rev. B* **34** 6690–4
- [30] Mueller D R, Clark C W, Ederer D L, Jia J J, O'Brien W L, Dong Q Y and Callcott T A 1995 *Phys. Rev. A* **52** 4457–61
- [31] Rubensson J-E, Lüning J, Eisebitt S and Eberhardt W 1997 *Appl. Phys. A* **28** 588–601
- [32] Suljoti E, de Groot F M F, Nagasono M, Glatzel P, Hennies F, Deppe M, Pietzsch A, Sonntag B, Föhlisch A and Würth W 2009 *Phys. Rev. Lett.* **103** 137401
- [33] Miyahara T, Hanyu T, Ishii H, Yanagihara M, Kamada T, Kato H, Naito K and Suzuki S 1986 *J. Phys. Soc. Japan* **55** 408–13
- [34] Henke B L, Gullikson E M and Davis J C 1993 *At. Data Nucl. Data Tables* **54** 181–342
- [35] Achkar A J, Regier T Z, Wadati H, Kim Y J, Zhang H and Hawthorn D G 2011 *Phys. Rev. B* **83** 081106
- [36] O'Brien W L, Jia J, Dong Q-Y, Callcott T A, Rubensson J-E, Mueller D L and Ederer D L 1991 *Nucl. Instrum. Methods Phys. Res. B* **56–57** 320–3
- [37] Okusawa M, Ichikawa K, Aita O and Tsutsumi K 1987 *Phys. Rev. B* **35** 478–81
- [38] Kowalczyk S P, Edelstein N, McFeely F R, Ley L and Shirley D A 1974 *Chem. Phys. Lett.* **29** 491–5
- [39] Sairanen O P, Aksela S and Kivimäki A 1991 *J. Phys.: Condens. Matter* **3** 8707–14
- [40] Knapp J A, Himpel F J and Eastman D E 1979 *Phys. Rev. B* **19** 4952–64
- [41] Yorikawa H 2011 *J. Electron Spectrosc. Relat. Phenom.* **184** 379–83
- [42] Kim S, Kim K and Min B I 2015 *Sci. Rep.* **5** 15052
- [43] Falkowski M, Doležal P, Duverger-Nédellec E, Chamoreau L M, Forté J, Andreev A V and Havela L 2020 *Phys. Rev. B* **101** 174110